

Constant effective mass across the phase diagram of high- T_c cuprates

W. J. Padilla,* Y. S. Lee, and M. Dumm†

Department of Physics, University of California at San Diego, La Jolla, CA 92093-0319.

G. Blumberg

Bell Laboratories, Lucent Technologies, Murray Hill, New Jersey 07974, USA.

S. Ono, Kouji Segawa, Seiki Komiya, and Yoichi Ando

Central Research Institute of Electric Power Industry, Komae, Tokyo 201-8511, Japan.

D. N. Basov

Department of Physics, University of California at San Diego, La Jolla, CA 92093-0319

We investigate the hole dynamics in two prototypical high temperature superconducting systems: $\text{La}_{2-x}\text{Sr}_x\text{CuO}_4$ and $\text{YBa}_2\text{Cu}_3\text{O}_y$ using a combination of DC transport and infrared spectroscopy. By exploring the effective spectral weight obtained with optics in conjunction with DC Hall results we find that the transition to the Mott insulating state in these systems is of the “vanishing carrier number” type since we observe no substantial enhancement of the mass as one proceeds to undoped phases. Further, the effective mass remains constant across the entire underdoped regime of the phase diagram. We discuss the implications of these results for the understanding of both transport phenomena and pairing mechanism in high- T_c systems.

PACS numbers: 74.25.Gz, 74.25.Kc, 74.72.Dn

At zero temperature in a Mott-Hubbard (MH) insulator, carriers are localized due to strong electron-electron interactions. In some systems long range antiferromagnetic (AF) order is favored due to superexchange.¹ Moving away from this ground state by heating or doping, a number of exotic behavior emerge.^{2,3} These include unconventional magnetic order⁴, pseudogap phenomena⁵, and high- T_c superconductivity (SC). To elucidate these complex forms of matter, it is necessary to clarify the origins of conduction as evolved from the undoped zero temperature state of the MH insulator. In fact, since the discovery of high- T_c SC this task has been widely regarded as one of the most fundamental problems in all of condensed matter physics.⁶ Here we study the only known class of MH systems to exhibit high- T_c superconductivity, the cuprates. Transport and infrared properties are presented for two prototypical families: $\text{La}_{2-x}\text{Sr}_x\text{CuO}_4$ (LSCO) and $\text{YBa}_2\text{Cu}_3\text{O}_y$ (YBCO). We show that the optical effective mass remains constant throughout the underdoped region of the phase diagram and discuss the implications of this enigma for both transport and superconductivity.

As a probe into the carrier dynamics of these two archetypal compounds we utilize a combination of DC transport and infrared spectroscopy. The optical measurements have been carried out from 1.2 meV to 6 eV (10 cm^{-1} to 50,000 cm^{-1}) in near normal reflectance geometry. Both the LSCO and YBCO samples are high quality de-twinned single crystals, the preparation of which was described previously in detail.⁷ Detwinned samples are especially important for YBCO to ensure that the a-axis data analyzed in this work are not contaminated by the contribution due to Cu-O chain segments. The optical conductivity $\sigma_1(\omega) + i\sigma_2(\omega)$ and complex dielectric func-

tion $\varepsilon_1(\omega) + i\varepsilon_2(\omega)$ was determined from the reflectance data^{8,9} and checked against direct ellipsometric measurements. This work encompasses the underdoped regime of the phase diagram from long range AF ordered insulators, to high- T_c SC compounds.

The real part of the conductivity $\sigma_1(\omega)$ is displayed in Fig. 1 (panels e-h) and shows the evolution of the doping trends. It has been established that the lowest electronic excitation in undoped crystals of different families of high- T_c superconductors is associated with a charge transfer (CT) gap at $\simeq 12000 \text{ cm}^{-1} = 1.5 \text{ eV}$.¹⁰ The data presented in Fig. 1 reveals the development of two distinct features in the intra-gap response upon carrier doping, in accord with the earlier results.^{10,11} The low-energy response is dominated by a Drude-like coherent contribution to the conductivity followed by a broad resonance in the mid-IR. We represent the dissipative part of the conductivity composed of two components as, $\sigma_1(\omega) = \omega_{pD}^2 \frac{\gamma_D}{\omega^2 + \gamma_D^2} + \omega_{pM}^2 \frac{\gamma_M \omega^2}{(\omega_M^2 - \omega^2) + \gamma_M^2 \omega^2}$, where ω_p^2 is the square of the plasma frequency for each term (subscripts D and M are for the Drude and MIR terms respectively), ω_M is the center frequency of the MIR term, γ_D and γ_M are the Drude and MIR damping terms respectively. With increasing doping the oscillator strength associated with both contributions is enhanced (this is further detailed in Fig. 2). The low-energy contribution to the conductivity is adequately described with the Drude expression (red regions in Fig. 1 f-h) revealing the metallic nature of the electronic transport even in AF-ordered phases.^{7,12,13} Approaching optimal doping at $T = T_c$, the two components in the conductivity merge and can no longer be unambiguously identified. Notably, both the LSCO and YBCO series reveal exactly the same trends.

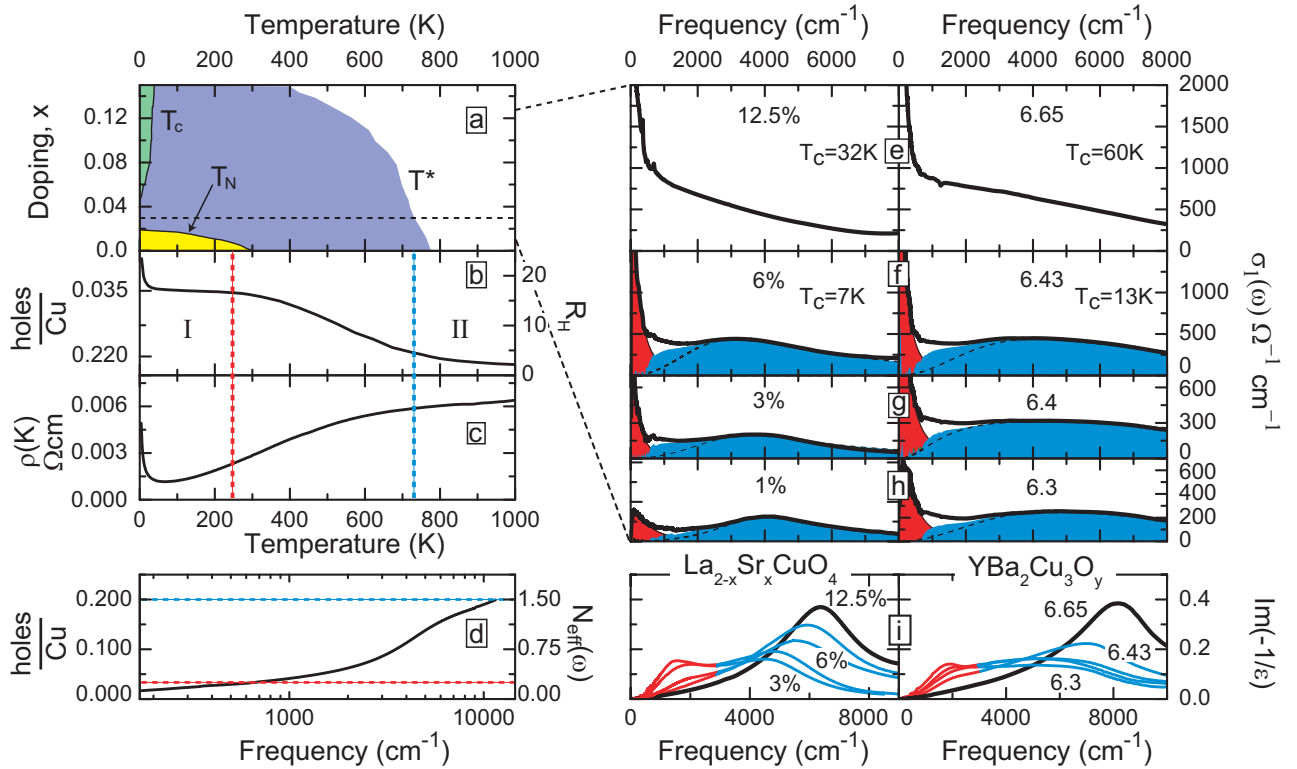


FIG. 1: (Color online). Optical data for YBCO and both optical and transport data for LSCO discussed in the context of the high- T_c phase diagram. Left panels are data for $x=0.03$ LSCO and right panels depict the low temperature optical conductivity as a function of doping for both LSCO and YBCO. Data in panels f-h are at $T=7$ K and at T just above T_c in panels e. Panel a: phase diagram with the values shown for LSCO; the yellow area is the long range AF region (denoted by T_N), the green area: superconducting region (marked by T_c), and the pseudogap region is denoted by T^* . To facilitate a direct comparison with the data, temperature is plotted on the horizontal axis and doping on the vertical axis. The Hall coefficient R_H (10^{-3} cm^3/C) displayed in panel (b) reveals two characteristic regimes (I and II). This is exemplified for the $x=0.03$ sample but similar behavior is found for all heavily underdoped crystals. These regimes can also be identified with significant regions in the DC resistivity corrected for thermal expansion (c). Panel d: the effective number of carriers, N_{eff} (10^6 $\Omega^{-1}\text{cm}^{-2}$), determined from the optical data as described in the text. Right panels: the real part of the conductivity at low temperature ($T=10$ K, except $T=T_c$ for e and f and $T=150$ K for $y=6.65$), displayed as black solid curves. Red colors signify fits using the standard Drude model. The blue area is a subtraction of the Drude fit from $\sigma_1(\omega)$ and is referred to as the “mid-infrared contribution” throughout the text. The resonant structure in the latter contribution can be adequately described with a Lorentzian oscillator (dashed lines). The loss function $[\text{Im}(-1/\epsilon)]$, panels (i), also clearly depicts two components (shown as red and blue curves) for dopings $x < 0.10$, $y < 6.65$, and the progression to a single component, (black solid curve) for higher dopings.

New insights into the nature of electronic transport in underdoped phases can be inferred from a combination of the $\sigma(\omega)$ results discussed above and the Hall and resistivity data obtained for nominally identical single crystals. We first note that in very underdoped crystals the behavior of the Hall coefficient is rather simple.¹³ This is exemplified for $x=0.03$ crystal (Fig. 1b). Indeed, R_H^{-1} is essentially independent of temperature below 300-400 K until the lowest temperatures where both transport and optics data are strongly influenced by Anderson localization.¹⁴ Moreover, the carrier density $n_H = R_H^{-1}$ extracted from this plateau is in fair agreement with an estimate based on the chemical composition of 0.035 holes per copper atom.^{7,13} The latter inference holds for other underdoped phases of both the LSCO and YBCO

series.^{7,15}

In order to establish parallels between transport and optics results it is customary to define the effective number of carriers $N_{eff}(\omega) = \int_0^\omega d\omega' \sigma_1(\omega')$ contributing to the conductivity below a cut-off frequency ω . The strength of the coherent contribution to the conductivity can be quantified either through the parameters of the Drude fit or by limiting the integration cut-off to 650 cm^{-1} . The results of the latter approach are displayed with the filled red symbols in Fig. 2. The coherent contribution amounts to approximately 20% of the total spectral weight below the CT excitation (Fig. 1d and open blue squares in Fig. 2). Inspecting the data in Fig. 2 one finds that both n_H and N_{eff}^{coh} reveal the same doping dependence in underdoped compounds where two com-

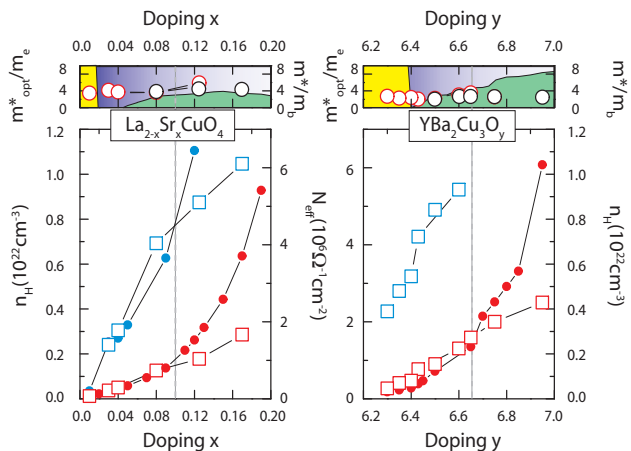


FIG. 2: (Color online). Top panels show the optical effective mass as determined by the methods described in the text. Red symbols are the mass determined using a combination of optics and transport (left axis labels), and the black symbols represent the mass determined within the extended Drude model (right labels). All methods produce consistent results and mass values which are doping independent over large regions of the phase diagram. The low temperature long range AF ordered phase is denoted by the yellow shaded area and SC region by the green area. Note that despite the formation of the AF regime near the Mott transition, there is no noticeable enhancement of the optical mass. Bottom panels show both the effective spectral weight from optics data (red and blue open squares) and the number of holes as determined by transport (red and blue dots).

ponent response can be identified in the IR data. With doping progressing towards optimal one witnesses a departure between the two results, again occurring in the same fashion for both the LSCO and YBCO series.

Encouraged by the close consistency between optics and Hall data in underdoped regime we evaluated the optical effective mass of mobile holes as $m_{Opt}^* = (R_H \times N_{eff}^{coh})^{-1}$. These mass values are plotted as the red symbols in the top panel of Fig. 2. At doping levels above a critical value ($x \sim 0.10$ for LSCO and $y \sim 6.65$ for YBCO) one cannot unambiguously separate the coherent component from the mid-IR background. Nevertheless, the mass enhancement over the band value can still be determined using solely optical data within the framework of the “extended Drude model” $\frac{m^*}{m_b} = -\frac{\omega_p^2}{4\pi} \frac{1}{\omega} \text{Im}[\frac{1}{\sigma(\omega)}]$ (black symbols in top panel of Fig. 2),¹⁶ and these are plotted as the black symbols in Fig. 2. Interestingly the two approaches produce consistent results. The key outcome of this analysis is that m_{Opt}^* is nearly doping independent in both LSCO and YBCO.

The topology of the Fermi surface in weakly doped cuprates is such that the masses calculated here reveal important dynamical characteristics of the electronic states in the nodal region, and are thus related to the nodal quasiparticle effective mass. Doping independent

m_{Opt}^* in both families of cuprates excludes the notion that carriers doped in MH system necessarily experience a divergence of m^* near the transition to an insulator.¹⁷ Although we are not aware of any direct inference of the effective mass for the cuprates from the specific heat data, an inspection of the doping dependence of linear coefficient γ supports our findings for m_{Opt}^* .^{18,19}

A theoretical analyses of the dynamics of mobile holes introduced into an antiferromagnet with the exchange energy J suggests that the mass divergence can be avoided.^{20,21,22} Nevertheless, the effective mass is still strongly renormalized by the ratio of t/J where t is the bandwidth. A common denominator in these models is that the motion of a hole in an AF background implies a continuous reorganization of the local spin environment. Since these processes are energetically costly they restrict carrier transport and enhance the effective mass with $t/J \sim 10$ in the Cuprates.²¹ The experimental situation for non-superconducting MH oxides is somewhat controversial. For example some materials indeed comply with the above expectations and show a strong increase of m^* when the Mott insulator boundary is approached both by varying concentration of dopants^{2,23,24} and hydrostatic pressure.²⁵ Other systems do not show such an enhancement.²⁶ Our data for high- T_c cuprates report, for the first time, a systematic study of the optical effective mass in this class of materials, and reveal relatively light masses. More importantly no noticeable changes in m_{Opt}^* are found despite the formation of long range AF ordered phases, and even in immediate proximity to the Mott insulating state.

It is instructive to discuss the constant effective mass result in conjunction with other universal trends of cuprates. Our observations imply that the development of the conducting state occurs primarily through an increase in the density of carriers, while the dynamical characteristics of mobile holes remain remarkably constant throughout the entire phase diagram. This conclusion is in accord with transport data^{7,18} and also supported by recent photoemission studies.²⁷ The latter work reports a gradual development of the Fermi arc and finds that the integrated weight varies proportionally to n with doping. Interestingly, measurements along the “nodal region” (the direction of $[0,0]$ to $[\pi, \pi]$ in k -space), find that the Fermi velocity also is insensitive to doping.²⁸ One conjecture reconciling all these observations is that the local environment of mobile charges in cuprates remains unaltered with doping and it is only the phase space occupied by hole rich regions that is progressively increasing. Some of these trends are also consistent with the variational analysis of doped holes in a resonant valence bonds insulator.²⁹

We now wish to highlight several unexpected features in the high temperature DC transport of very underdoped crystal relating these features to the IR results. The Hall number $n_H = R_H^{-1}$ shows a marked increase at $T > 300 - 400$ K with a new plateau emerging above 800-900 K as exemplified for $x=0.03$ LSCO crystal in

Fig. 1b. An increase in the Hall number occurs primarily between regions I and II (Fig. 1 b) and appears to impact the T dependence of the resistivity $\rho(T)$, Fig. 1 (c). Indeed the rapid growth of the resistivity with T in regime I is followed by a nearly T-independent resistivity in regime II.³⁰ The inverse resistivity in the saturated region is in quantitative agreement with the magnitude of conductivity in at mid-IR frequencies. It is known that the coherent Drude-like feature clearly seen in the low-T data in Fig. 1 significantly broadens with increasing T and can no longer be discriminated from the incoherent mid-IR background as T is elevated to 400 K.³¹ We speculate that the transformation of $\sigma(\omega)$, resistivity and n_H at elevated temperatures may all be of common origin. At these high temperatures quasiparticles residing on the Fermi arcs lose their identity and it is no longer possible to distinguish the role of these excitations in the transport properties from that of an “incoherent background”. One corollary of the results reported here is that the magnitude of m_{Opt}^* reported in Fig. 2 remains unchanged if

this value is extracted from the total spectral weight (below the charge transfer absorption) in combination with n_H at 800-900 K.

In conclusion, we have investigated the optical mass associated with the response of nodal quasiparticles across the underdoped regime of two prototypical high- T_c superconducting families. Our results establish an alternative route for the Mott transition in this class of materials without the usual mass divergence or enhancement. One implication of a constant effective mass is that transport in high- T_c cuprates is governed by excitations topologically compatible with an antiferromagnetic background. Specific schemes permitting a constant effective mass include spin-charge separation²¹ and electronic phase separation.³² Both scenarios propose unconventional and exotic explanations of high- T_c superconductivity which depart from the standard BCS prescription.

-
- * Present address: Los Alamos National Laboratory, MS G756, MST-CINT, Los Alamos, NM 87545.; Electronic address: willie@lanl.gov
- † Present address: 1. Physikalisches Institut, Universität Stuttgart, 70550 Stuttgart, Germany
- ¹ P. W. Anderson, Phys. Rev. **115**, 2 (1959).
- ² M. Imada, A. Fujimori, Y. Tokura, Rev. Mod. Phys. **70**, 1039 (1998).
- ³ A. Georges, G. Kotliar, W. Krauth, M. J. Rozenberg, Rev. Mod. Phys. **68**, 13 (1996).
- ⁴ K. Yamada, C. H. Lee, K. Kurahashi, J. Wada, S. Wakimoto, S. Ueki, H. Kimura, Y. Endoh, S. Hosoya, G. Shirane, R. J. Birgeneau, M. Greven, M. A. Kastner, Y. J. Kim, Phys. Rev. B **57**, 6165 (1998).
- ⁵ T. Timusk, B. Statt, Rep. Prog. Phys. **62**, 61 (1999).
- ⁶ J. Orenstein, A. J. Millis, Science **288**, 468 (2000).
- ⁷ Y. Ando, A. N. Lavrov, Seiki Komiya, Kouji Segawa, X. F. Sun, Phys. Rev. Lett. **87**, 017001 (2001).
- ⁸ This was obtained by a Kramer-Kronig transformation of the data after extrapolation to low and high energies.
- ⁹ F. Wooten, *Optical Properties of Solids* (Academic Press, New York, 1972).
- ¹⁰ D. B. Tanner, T. Timusk, Infrared Properties of High T_c Superconductors, in *Physical Properties of High Temperature Superconductors III*. D.M. Ginsberg, editor, (World Scientific, Singapore, 1992).
- ¹¹ S. Uchida, T. Ido, H. Takagi, T. Arima, Y. Tokura, S. Tajima, Phys. Rev. B **43**, 7942 (1991).
- ¹² For $x=0.01$ and 0.03 LSCO crystals we used localization modified Drude formula accounting for a shift of the Drude feature to finite frequency: a hallmark of Anderson localization in $\sigma(\omega)$. While Anderson localization modifies the response of the system at lowest frequencies it is nevertheless appropriate to classify these crystals as metallic. Notably, a significant electronic spectral weight extends down to the lowest energies without any indications for a gap in the density of states. The AF-ordered YBCO crystal with $y=6.3$ reveals a conventional Drude response, at

- lower dopings we observed a Anderson localization feature in YBCO compounds as well.
- ¹³ Y. Ando, Y. Kurita, S. Komiya, S. Ono, K. Segawa, Phys. Rev. Lett. **92**, 197001 (2004).
- ¹⁴ Both the resistivity and the Hall data for very light dopings are influenced by carrier localization [upturns in both $R_H(T)$ and $\rho(T)$]. Localization trends are also evident in the $\sigma(\omega)$. This behavior is not analyzed further here.
- ¹⁵ K. Segawa, Y. Ando, Phys. Rev. B **69**, 104521 (2004).
- ¹⁶ The plasma frequency is determined from the minimum in the reflectivity, with typical values for the Cuprates studied here around 1eV. For a detailed description of Extended Drude analysis see: A. V. Puchkov, D. N. Basov, T. Timusk, J. Phys.: Condens. Matter **8**, 10049 (1996).
- ¹⁷ W. F. Brinkman, T. M. Rice, Phys. Rev. B **2**, 4302 (1970).
- ¹⁸ K. Kumagai, T. Suzuki, Y. Taguchi, Y. Okada, Y. Fujishima, Y. Tokura, Phys. Rev. B **48**, 7636 (1993).
- ¹⁹ J. W. Loram, K. A. Mirza, W. Y. Liang, J. Osborne, Physica C **162-164**, 498 (1989).
- ²⁰ S. A. Trugman, Phys. Rev. B **37**, 1597 (1988).
- ²¹ C. L. Kane, P. A. Lee, N. Read, Phys. Rev. B **39**, 6880 (1989).
- ²² S. Sachdev, Phys. Rev. B **39**, 12232 (1989).
- ²³ Y. Tokura, Y. Taguchi, Y. Okada, Y. Fujishima, T. Arima, K. Kumagai, Y. Iye, Phys. Rev. Lett. **70**, 2126 (1993).
- ²⁴ Y. Fujishima, Y. Tokura, T. Arima, S. Uchida, Phys. Rev. B **46**, 11167 (1992).
- ²⁵ S. A. Carter, T. F. Rosenbaum, P. Metcalf, J. M. Honig, J. Spalek, Phys. Rev. B **48**, R16841 (1993).
- ²⁶ T. Katsufuji, Y. Taguchi, Y. Tokura, Phys. Rev. B **56**, 10145 (1997).
- ²⁷ T. Yoshida, X. J. Zhou, T. Sasagawa, W. L. Yang, P. V. Bogdanov, A. Lanzara, Z. Hussain, T. Mizokawa, A. Fujimori, H. Eisaki, Z.-X. Shen, T. Kakeshita, S. Uchida, Phys. Rev. Lett. **91**, 27001 (2003).
- ²⁸ X. J. Zhou, A. Lanzara, P. V. Bogdanov, S. A. Kellar, K. M. Shen, W. L. Yang, F. Ronning, T. Sasagawa, T. Kakeshita, T. Noda, H. Eisaki, S. Uchida, C. T. Lin, F.

- Zhou, J. W. Xiong, W. X. Ti, Z. X. Zhao, A. Fujimori, Z. Hussain, Z.-X. Shen, *Nature* **423**, 398 (2003).
- ²⁹ A. Paramekanti, M. Randeria, N. Trivedi, *Phys. Rev. Lett.* **87**, 217002 (2001).
- ³⁰ Although the resistivity shown in Fig. 1(c) continues to slowly increase between regions I and II, the curvature inflection point occurs at approximately 300K. Thus the onset of resistivity saturation occurs simultaneously with the increase in the number of carriers.
- ³¹ K. Takenaka, J. Nohara, R. Shiozaki, S. Sugai, *Phys. Rev. B* **68**, 134501 (2003).
- ³² V. J. Emery, S. A. Kivelson, O. Zachar, *Phys. Rev. B* **56**, 6120 (1997).